Rock Mechanics and Rock Engineering
https://doi.org/10.1007/s00603-022-02870-3

TECHNICAL NOTE

Fractal Characteristics of Drilling Particle Size Distribution of Shale: A Laboratory Scale Investigation

Xiaofeng Yang[1] · Aiguo Nie[1] · Derek Elsworth[2] · Jiaheng Zhou[1] · Ying Tao[1]

Received: 30 September 2021 / Accepted: 30 March 2022
© The Author(s), under exclusive licence to Springer-Verlag GmbH Austria, part of Springer Nature 2022

Highlights

- The fractal particle size distribution (PSD) theory is used to characterize the particles produced in shale drilling.
- Fractal dimension comprehensively reflects the characteristic particle size and features of the distribution of the drilling PSD.
- Wear effect produces nano-particles with a volume of ~1.88–3.76% during the particles transport process which increases the dissipation of drilling energy.
- Higher rotation rate increases the proportion of coarse particles and is conducive to reducing wear effect.

Keywords Rock drilling · Particle size distribution · Fractal dimension · Operating parameters

List of symbols

PSD	Particle size distribution
d_{50}	Medium particle size
Z	Rate of rotation
T	Rate of penetration
ϕ	Diameter of cylindrical sample
d	Particle size
N	Number of particles
D	Fractal dimension
K	Fitting constant
V	Accumulative volume of particles
β	Shape factor
$d_{\min}$	Minimum particle size
$d_{\max}$	Maximum particle size
P	Percent by volume
d_i	Specific particle size
φ	Dispersion of PSD
R_d	Span of particle sizes
P_d	Maximum frequency
d_{MPS}	Mean particle size
d_e	Absolute particle size
CI	Coarseness index
n	Uniformity of PSD
Φ	Phi-size
Φ_{16}, Φ_{50}, Φ_{84}	16Th, 50th, and 84th phi-size
$P_{\mathrm{re}}(d)$	Cumulative percentage of particles
R	Linear correlation coefficient
ROP	Rate of penetration
I	Savage number
$\dot{\gamma}$	Characteristic shear rate
d_p	Characteristic particle size
P_f	Pressure of granular flow
ρ_p	Bulk density
σ, τ	Normal stress and shear stress
μ_{eff}	Effective friction coefficient
$u(\vec{r})$	Velocity distribution
$\vec{r}$	Position vector
V_W	Velocity of mobile wall

✉ Xiaofeng Yang
xfyang@cumtb.edu.cn

[1] School of Mechanics and Civil Engineering, China University of Mining and Technology, Beijing 100083, China

[2] Department of Energy and Mineral Engineering, EMS Energy Institute and G3 Center, Pennsylvania State University, University Park, PA, USA

1 Introduction

Rock drilling is an engineering activity widely used in mining and civil applications, such as the exploration and development of oil, gas and other geological resources and in tunneling (Hood and Alehossein 2000; Kwon et al. 2014; Munoz et al. 2016; Li and Weijermars 2019). Rock drilling

Published online: 11 June 2022

includes a common process where comminution and the cutting of rocks into fragments or particles is coupled with their continuous discharge from the zone of excavation. The produced particles reflect the performance of rock failure and fragmentation, exerting an important influence on energy consumption, drilling resistance and efficiency (Dunatunga and Kamrin 2017; Okorie 2017).

Although the formation mechanisms and effects on the resulting comminuted products are complex, the drilling process and properties of the cuttings are somewhat understood and reported in the literature. The link between the cutting force frequencies and the sizes of the produced chips (Rojek et al. 2011) and the effect of hydrostatic pressure on the morphology of the cuttings (Block and Jin 2009) has been investigated using DEM simulations of tool–rock interaction processes. The size and shape of rock particles exert a significant impact on the heat dissipation, with higher proportion of coarse particles and lower roundness impeding heat dissipation (Baumann and Zunft 2015; Jiang and Liu 2017). Additionally, the clogging of particles may raise the temperature of the drill bit and greatly reduce bit-life and drilling efficiency (Yang et al. 2014; Patrik et al. 2016). In the borehole wall of shale gas reservoir development, it has been found that the size and distribution of drilling particles also have an effect on rock permeability since particles fill the cracks and block seepage channels (Dahi-Taleghani and Olson 2011; Ma 2015; Fang et al. 2017). Moreover, the rheology of the drilling fluid is closely related to drilling particle size distribution. Gamwo and Kabir (2015) found that finer particles enhance the fluidity of drilling fluids and reduce flow resistance. Therefore, the particle size distribution (PSD) of drilling products inherently relates to the productivity and cost of shale gas development, and it is becoming widely studied.

The PSD reflects the process of particle crushing, or particle breakage (Muir Wood and Maeda 2007; Wang et al. 2019; Zhou et al. 2019). The PSD is commonly measured by sieving or image analysis, plotted as a histogram and as a frequency or cumulative curve, and further analyzed by mathematical and statistical methods. Statistical analysis mainly adopts a series of characteristic parameters to represent the entire PSD through some convenient index parameter, such as representative size (median particle size, mean particle size, effective particle size, constrained particle size), PSD width or coarseness index (Yang et al. 2021). Ersoy and Waller (1997) adopted medium particle size d_{50} from PSD data to quantitatively analysis the drilling detritus, and established a relation between particle size and cutter size or wear of the polycrystalline diamond cutters PDCs. Altindag (2003) investigated the relationship between penetration rate and coarseness index and mean particle size based on PSD analysis, and proposed a prediction model for penetration rate. However, Gamwo and Kabir (2015) found it is difficult to establish a quantitative relationship between PSD and drilling operating parameters using the d_{50} index (or other average sizes), alone. Thus, mathematical methods are widely adopted, and PSD has been proposed in exponential, logarithmically normal and multi-peak mass frequency distributions as well as fractal (power) distribution models (Xu and Liu 1999; Blair 2004; Lee et al. 2014; Li et al. 2017).

Fractal theory is widely used to quantify the size distribution of geotechnical granular materials, since it has an advantage in describing complex and disordered objects and phenomena in nature (Perfect 1997; Xu et al. 2016; Huang et al. 2017). In defining grain crushing processes, Turcotte (1986) argued that any initial distribution of particles will tend towards a self-similar distribution. This precept that the PSD of comminuted particles tends to be fractal is widely accepted (McDowell et al. 1996; Einav 2007). Quartz grains produced from lateral compression tests have been demonstrated to exhibit relatively strict self-similarity with fractal dimensions > 2.2 (Zhang et al. 2015). Demolition waste has been shown to have a fractal dimension in the range 2.50–2.60, with a fractal dimension of 2.5 corresponding to the highest maximum dry density (Xu 2018). Moreover, fractal fragmentation theory has been adopted to describe the fragmentation process and a relationship among specific energy, breakage probability and particle size has been derived (Xu and Wang 2017). Xu (2017) also established a relation between the applied stress, fracture energy and fractal dimension of marble particles based on drop hammer tests. The relationships between loading conditions and resulting PSDs, for various materials, have been defined, based on fractal theory. Thus, fractal theory has been established to possess a theoretical basis and offers an alternative approach in studying the PSDs resulting from rock drilling, with only a few published studies conducted to determine the fractal characteristic of drilling particles and its relationship with drilling efficiency.

The objective of this study is to investigate the characteristics of rock drilling PSDs based on fractal theory and define their effect on drilling efficiency. A series of drilling tests were conducted on shales and the fractal behavior of the resulting particles was investigated. The relationships between fractal dimension of the PSDs and drilling

Table 1 Mechanical and physical properties of shale samples (averaged measured)

Uniaxial compressive strength (MPa)	Shear strength (MPa)	Shear angle (°)	Density 10^3 kg/m^3
139	56	27	2.59

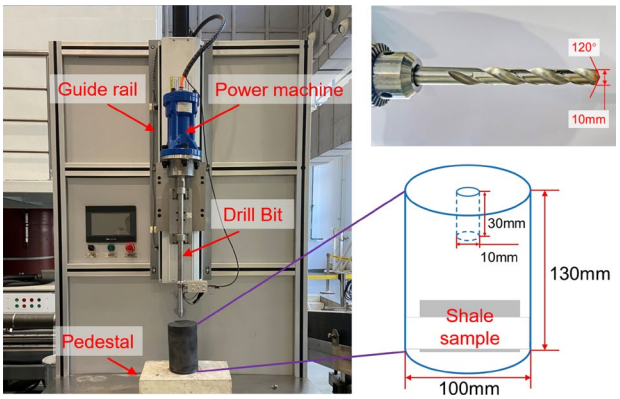

Fig. 1 Laboratory drilling system

Table 2 Drilling operational parameters

Penetration rate T		Rotation rate Z	
Serial number	Penetration (mm/s)	Serial number	Rotation (rpm)
T1	0.75	Z1	600
T2	0.85	Z2	900
T3	1.00	Z3	1250
T4	1.20	Z4	1750
T5	1.50	Z5	2600

operating parameters were investigated to optimize drilling efficiency.

2 Experimental Procedures and Materials

2.1 Rock Samples

Drilling tests were carried out on shale recovered from the Fuling shale gas field in southwest China. The principal mechanical properties of the samples were measured according to ISRM standards. A minimum of five repeated tests were completed, with the results showing good repeatability and inferring homogeneity. The physical and mechanical properties of the samples are given in Table 1. The shales were cut into cylindrical samples (ϕ100 mm × 130 mm).

2.2 Rock Drilling Tests

A laboratory rig was constructed to simulate the dynamic conditions of rock drilling, as shown in Fig. 1. The drilling system comprises a modified electric drill (1 kW) in a tower press and with a longitudinal bit feed mechanism, a twist drill, and an operating console linked to an external computer. The bit of the twist drill is made of carbide YG8 with a bit diameter of 10 mm and a wedge angle of 120°.

In the dry drilling procedure, the drill bit was controlled by a set rate of both rotation and penetration. A servo-control module controls the set rates of rotation Z ranging from 600 to 2600 rpm and penetration T from 0.75 to 1.50 mm/s. Each set rate was at one of five levels as given in Table 2. Each level of rotation was combined with a single penetration rate to comprise a single test. Thus, a suite of 25 drilling tests were carried out. The drilling depth was set to 30 mm by adopting an appropriate drilling

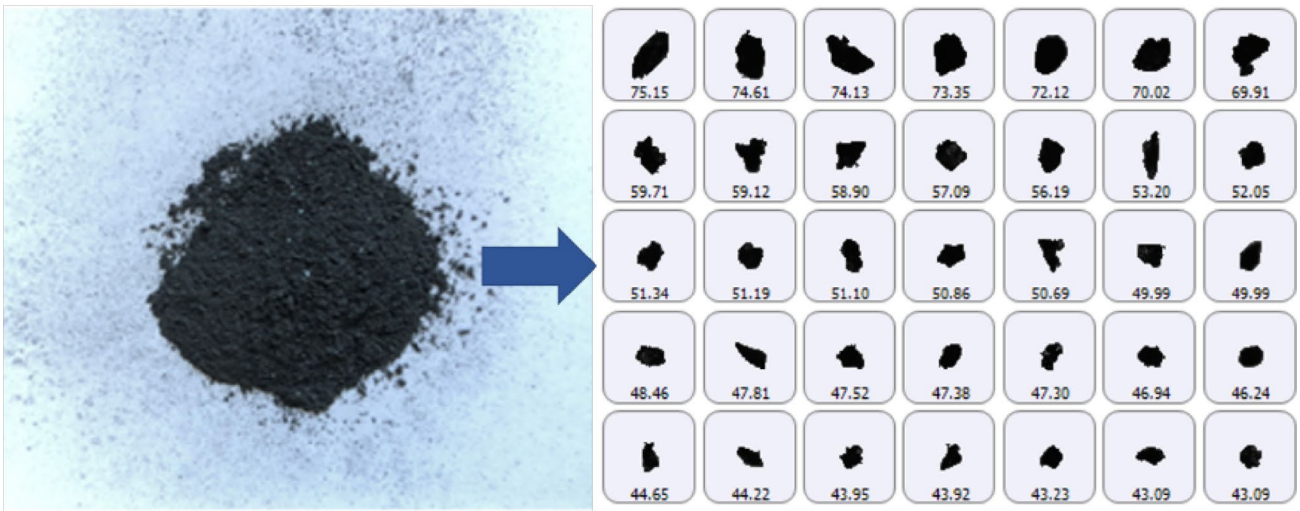

Fig. 2 The morphologies of drilling particles (particle size (μm) is noted under each image)

time in each test. The rock sample was fixed by a ring clamp fixed on the pedestal. Before testing, the samples were lubricated on the basal and lateral sides to reduce the effect of friction. After each test, the generated drilling particles were carefully collected (typically ~ 2 cm^2) for particle size tests.

2.3 Particle Size Tests

The drilling products are powders generally of micrometer size, as shown in Fig. 2. The PSDs of the drilling particles were measured by a laser diffraction particle size analyzer Marvern Mastersizer 3000, as well as an image analyzer Malvern Morphology G3SE (Malvern Instruments, Malvern Company, UK). Compared with the measurement of traditional sieve test, the volume rather than mass proportions of particle fractions are obtained by the instruments. Moreover, the measured PSDs had more subtle size fractions, so that statistical quantities were available to accurately analysis the rock drilling and breakage.

3 Fractal Characteristics of Drilling PSD

3.1 Fractal Model of PSD

Fractal theory is now a fundamental topic in many research fields, widely accepted as a descriptive tool of physical systems in rock engineering. Once a fractal distribution of drilling particles is generated, the number of particles with the size larger than d is defined as (Turcotte 1986)

$$N(>d) = Kd^{-D} \tag{1}$$

where D is the fractal dimension of the particle size, $N(>d)$ is the total number of particles larger than diameter d and K is the fitting constant. The fractal dimension of the particle size ranges from 1.0 to 3.0 (Bourrous et al. 2016). The accumulative volume of particles is more readily measured than the specific number, with the cumulative volume V is related to the fractal number, and given as

$$V(\leq d) = \int_{d_{\min}}^{d} \beta d^3 \mathrm{d}N, \tag{2}$$

where the incremental number $\mathrm{d}N = KDd^{-D-1}$, derived by Eq. (1). $V(\leq d)$ is the volume of particles finer than d, β is the shape factor. Equation (2) is thus rewritten as

$$V(\leq d) = \frac{K\beta}{3-D}\left(d^{3-D} - d_{\min}^{3-D}\right). \tag{3}$$

The percent finer by volume $P(\leq d)$, is calculated from $P(\leq d) = V(\leq d)/V(\leq d_{\max})$, and is given as

$$P(\leq d) = \frac{d^{3-D} - d_{\min}^{3-D}}{d_{\max}^{3-D} - d_{\min}^{3-D}}, \tag{4}$$

where the maximum particle size $d_{\max}$ is at millimeter-level and the minimum particle size $d_{\min}$ at submicron level, i.e. $d_{\min} \ll d_{\max}$. The percent finer by volume may be simplified as

$$P(\leq d) = \left(\frac{d}{d_{\max}}\right)^{3-D} \tag{5}$$

Taking the logarithm of both sides of Eq. (5) enables this distribution to be rewritten as

$$\log P(\leq d) = (3-D)\log\left(\frac{d}{d_{\max}}\right). \tag{6}$$

The fractal dimension of the drilling particle size can be calculated using Eq. (6), based on the fitting method. The required data can, therefore, be recovered from the measured PSDs.

For the fitting computation, the span of particle sizes $I = [0.314,1110]$ (μm) was considered based on the measurement results. I is partitioned into seven subintervals $I = [d_i, d_{i+1}]$, $i = 1,2\ldots,7$. d_i is the specific particle size and was used to calculate D. And $\log[d_{i+1}/d_i]$ is a constant necessary to construct a new measure where the fitting computation can take advantage of data potential (Montero 2005). Subintervals according to screening accuracy are given as [0.314–1.13] μm, [1.13–3.55] μm, [3.55–11.2] μm, [11.2–35.3] μm, [35.5–111] μm, [111–352] μm, [352–1110] μm. Therefore, 6–7 data points are available to accurately characterize the D values of the drilling-generated particles.

3.2 Dispersion and Fractal Dimension

PSD can be analyzed by graphical methods. A frequency PSD curve defines a peak, similar to a Gaussian curve (see Fig. 3b). We propose a straightforward description of the characteristic shape of the drilling-generated PSD, by drawing a triangular outline of the frequency distribution and covering the abscissa axis. The triangular outline of the PSD describes not only the key graphical features but also the degree of dispersion of the particle sizes, since the base of the triangle corresponds to the range of particle sizes and the height of the maximum frequency. Considering that the PSD is always plotted on a logarithmic scale, we define the dispersion φ of the PSD as the ratio between the span of particle sizes on the logarithmic scale R_d and the maximum

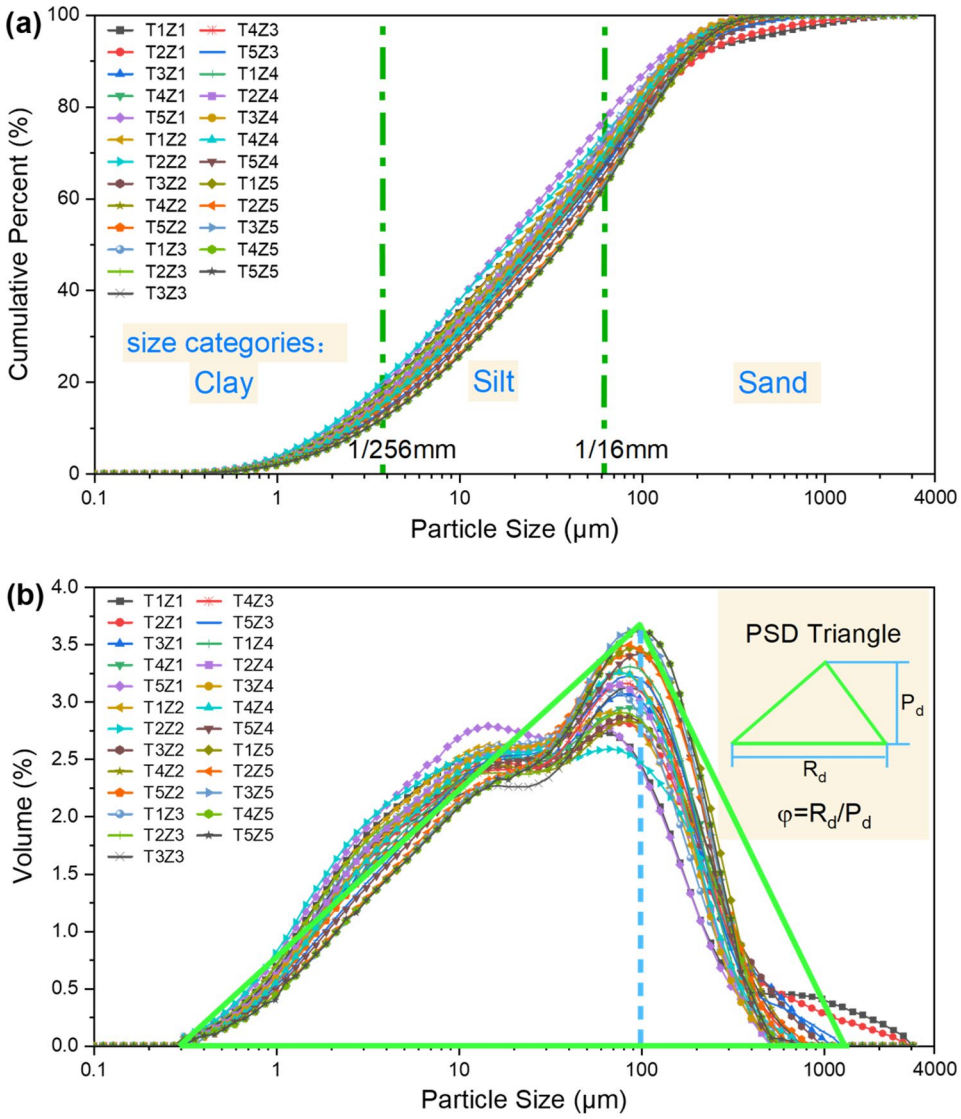

Fig. 3 Particle size distribution of drilling particles. **a** cumulative PSD curves and **b** frequency PSD curves

frequency P_d. Therefore, φ can be simply calculated from the base–height ratio of the PSD triangle, as

$$\varphi = \frac{R_d}{P_d} = \frac{\log d_{\max} - \log d_{\min}}{P_{\max}}, \tag{7}$$

where $P_{\max}$ is the maximum volume of a certain particle size (in decimal form). Equation (7) can be transformed into

$$\varphi = \frac{\log(d_{\max}/d_{\min})}{P_{\max}}. \tag{8}$$

Equation (8) indicates that φ is related to the ratio of the maximum to minimum particle size, and φ is a dimensionless number. Higher dispersion φ indicates a wider range and a smaller frequency amplitude of a PSD, defining a more dispersive distribution.

It is found that dispersion has a quantitative relation with fractal dimension. When $d_{\min}$ is inserted into Eq. (6), a relationship between φ and D can be thus established as

$$\varphi = \frac{\log P(d_{\min})}{(D-3)P_{\max}}, \tag{9}$$

where $P(d_{\min})$ is the volume percent of the particles with minimum size. Since $P(d_{\min}) < 1$ is always true, φ is positively related to D. It indicates that the dispersion of the PSD has an intrinsic connection with its fractal behavior.

4 Results and Discussion

4.1 PSD of Drilling Particles

Two types of PSD, cumulative and frequency distribution curves, for drilling products, are investigated. Figure 3a shows that the particles are mainly in the range 0.357–1110 μm and can be divided into three major size categories as clay (< 1/256 mm), silt (1/256–1/16 mm), and sand (1/16–2 mm) according to the Udden-Wentworth scale (Wentworth 1922). Particles in different size categories have different surface energies, reflecting the energy consumption and formation mode of particles during the drilling process. The distinction among these size categories is convenient to study the complex mechanisms of particle generation. Figure 3b shows that all frequency distribution curves are peaked in-shape with particle sizes concentrated in the range of 100 μm. This graphical shape is subsequently studied. Then, some characteristic parameters and mathematical models are adopted to further analyze the PSDs.

4.2 Fractal Dimension and Related PSD Parameters

The main parameters describing the PSD of drilling products, including representative sizes (median (d_{50}), mean (d_{MPS}) and absolute (d_e) particle size), coarseness index (CI), uniformity (n), dispersion (φ), and fractal dimension (D) are investigated.

Median particle size d_{50} denotes the size defining 50% of particles are finer and 50% is coarser than this diameter on the cumulative PSD. Mean particle size d_{MPS} is the arithmetic average of all particle diameters, calculated by Eqs. 10–12 (Mohammadi et al. 2019).

$$\Phi = -\log_2 d \tag{10}$$

$$M = \frac{\Phi_{16} + \Phi_{50} + \Phi_{84}}{3} \tag{11}$$

$$d_{\mathrm{MPS}} = 1/2^{M}, \tag{12}$$

where Φ is the phi-size proposed by Krumbein (1934), who adopted the logarithmic phi scale to describe rock PSDs. Thus, Φ_{16}, Φ_{50} and Φ_{84} are 16th, 50th, and 84th percentile values recovered from the cumulative PSD curve.

Coarseness index (CI) is a dimensionless number that expresses the size distribution of rock debris, recovered from traditional sieving tests (Roxborough and Rispin 1973). The CI is derived by using the sum of the percentages of the residue left on each successive sieve set. The value of CI is mainly affected by the finer fractions, since larger percentages correspond to smaller sieve sizes. CI depends strongly on the number of size fractions and sieve sizes used. Thus, the same size subintervals for all tests were used to calculate CI. A typical example of a CI calculation is given in Table 3, and the selected size subintervals are also shown.

The absolute particle size and uniformity are derived from the Rosin–Rammler distribution function of the PSD (Rosin and Rammler 1933), which is expressed as

$$P_{re}(d) = 100 \exp\left(\frac{-d}{d_e}\right)^{n} \tag{13}$$

$$\log\left[\ln(100/P_{re}(d))\right] = n\log d - n\log d_e, \tag{14}$$

Table 3 Calculation of CI depending on the selected size subintervals (example number: T3Z1)

Size subinterval (μm)	Volume (%)	Cumulative volume (%)
+ 1110	0	0
− 1110 + 352	2.93	2.93
− 352 + 111	15.4	18.33
− 111 + 35.3	26.22	44.55
− 35.3 + 11.2	22.51	67.06
− 11.2 + 3.55	18.22	85.28
− 3.55 + 1.13	11.23	96.51
− 1.13	3.49	100
Coarseness index (CI)		∑ = 414.66

Table 4 Data for Rosin–Rammler plot (example number: T4Z3)

Sieve size d (μm)	log d	$P_{\mathrm{re}}(d)$ (%)	log[ln(100/$P_{\mathrm{re}}(d)$)]	$d_e(d_{63.2})$	n	R
1110	3.045	0.01	0.964	51.8	0.770	0.992
352	2.547	1.37	0.632			
111	2.045	17.36	0.243			
35.3	1.548	44.29	− 0.089			
11.2	1.049	66.17	− 0.384			
3.55	0.550	84.92	− 0.787			
1.13	0.053	96.63	− 1.465			
0.314	− 0.503	100.00				

Table 5 Representative sizes (d_{50}, d_{MPS}, d_e) and coarseness index (CI) of PSDs for all drilling tests

Test number	d_{50}	d_{MPS}	d_e	CI	Test number	d_{50}	d_{MPS}	d_e	CI
T1Z1	23.6	19.68	40.71	402.65	T4Z3	30.0	23.83	49.97	410.74
T2Z1	29.1	22.55	49.83	415.35	T5Z3	33.4	26.67	54.01	420.95
T3Z1	30.5	24.69	50.86	414.66	T1Z4	31.2	24.42	50.36	412.05
T4Z1	27.8	22.90	51.80	406.76	T2Z4	26.2	21.34	42.98	400.82
T5Z1	19.9	17.38	32.65	384.19	T3Z4	27.5	22.23	44.83	404.43
T1Z2	23.5	19.94	39.25	395.41	T4Z4	29.0	23.21	47.03	408.65
T2Z2	20.9	18.46	36.22	388.46	T5Z4	35.7	27.65	56.91	422.19
T3Z2	28.1	23.10	48.53	410.06	T1Z5	41.3	30.99	62.97	431.44
T4Z2	27.3	22.91	47.70	407.58	T2Z5	39.8	30.06	60.42	429.23
T5Z2	31.8	24.67	50.31	414.17	T3Z5	41.1	30.53	62.03	430.38
T1Z3	25.1	20.58	40.95	398.39	T4Z5	41.7	30.87	63.67	431.32
T2Z3	26.4	21.73	45.74	402.84	T5Z5	42.4	31.00	63.60	431.36
T3Z3	30.7	23.94	52.33	411.17					

where $P_{re}(d)$ is the cumulative percentage of particles larger than size d, n is a constant describing the uniformity of the PSD, referred to as uniformity. d_e is the absolute particle size. This model is able to characterize a PSD with due consideration of the overall distribution, and has been applied to many other granular materials (Gupta and Yan 2006; Abu Bakar and Gertsch 2013). n is calculated using Eq. (14), by plotting 'log[ln(100/$P_{re}(d)$)]' versus 'log d' and fitting with a straight line. The slope of this linear fit is equal to n. d_e is the size at which 63.2% of the particles are smaller (or $P_{re}(d) = 36.8$, derived from Eq. (14) when $d = d_e$), and may be recovered directly from the measured PSD. The calculation method of n and d_e is given in Table 4 as an example, and the results for all tests are summarized in Table 5.

The calculated results of fractal dimensions for all drilling tests are given in Table 6 (R is the linear correlation coefficient in the fitting plots based on Eq. (6)). D values are distributed in the range of 2.376–2.497. In the most practical cases involving the breakage (or fragmentation) of rocks and granular materials, the ultimate distribution generally follows a fractal model with a D of ~ 2.5–2.6 (Simo and Ju 1987; Steacy and Sammis 1991). This indicates that the shale particles in this drilling tests have a higher degree of breakage.

Data of the evaluated D, CI and representative sizes for all tests are plotted in Fig. 4. This shows a negative linear relation between D and d_{50}, d_{MPS}, d_e, CI, respectively. The representative sizes and CI reflect the relative proportion of finer and coarser fractions, and their values decrease with the increase of fine particles. D values show a significant positive correlation with the proportion of fine particles (Tyler and Wheatcraft 1992; Gui et al. 2010; Zhao et al. 2017) and, therefore, D generally shows a negative correlation with the representative sizes and CI of drilling PSD. This linear relation may be used to directly estimate fractal dimension from representative sizes or coarseness index.

The calculated results of uniformity n and dispersion φ of PSD and their relationships with D are plotted in Fig. 5. It is apparent that n decreases and φ increases with an increase in D. Fractal dimension of the particle size distribution is one form of a capacity dimension as it quantifies how densely the fractal occupies the metric space in which it lies (Xu 2005). Particles with higher dispersion or lower uniformity (such as a broad/good particle grading) are readily densely packed and that corresponds to a higher D. Thus, that fractal dimension always has a strong correlation with the dispersion or uniformity of the PSD and as such reflects the packing density of the particles.

Fractal dimension is proposed to represent an important characteristic parameter of the PSD of the drilling-generated products, considering that it correlates with

Table 6 Fractal dimensions and fitting coefficients of drilling particles for all tests

Penetration (mm/s)	Rotation (rpm)									
	Z1		Z2		Z3		Z4		Z5	
	D	R	D	R	D	R	D	R	D	R
T1	2.472	0.933	2.459	0.937	2.450	0.9396	2.423	0.947	2.380	0.955
T2	2.449	0.942	2.497	0.937	2.472	0.9421	2.442	0.941	2.379	0.951
T3	2.446	0.947	2.454	0.941	2.461	0.9461	2.431	0.942	2.376	0.954
T4	2.452	0.946	2.459	0.942	2.441	0.9444	2.422	0.942	2.382	0.956
T5	2.486	0.935	2.418	0.947	2.410	0.9483	2.399	0.951	2.383	0.955

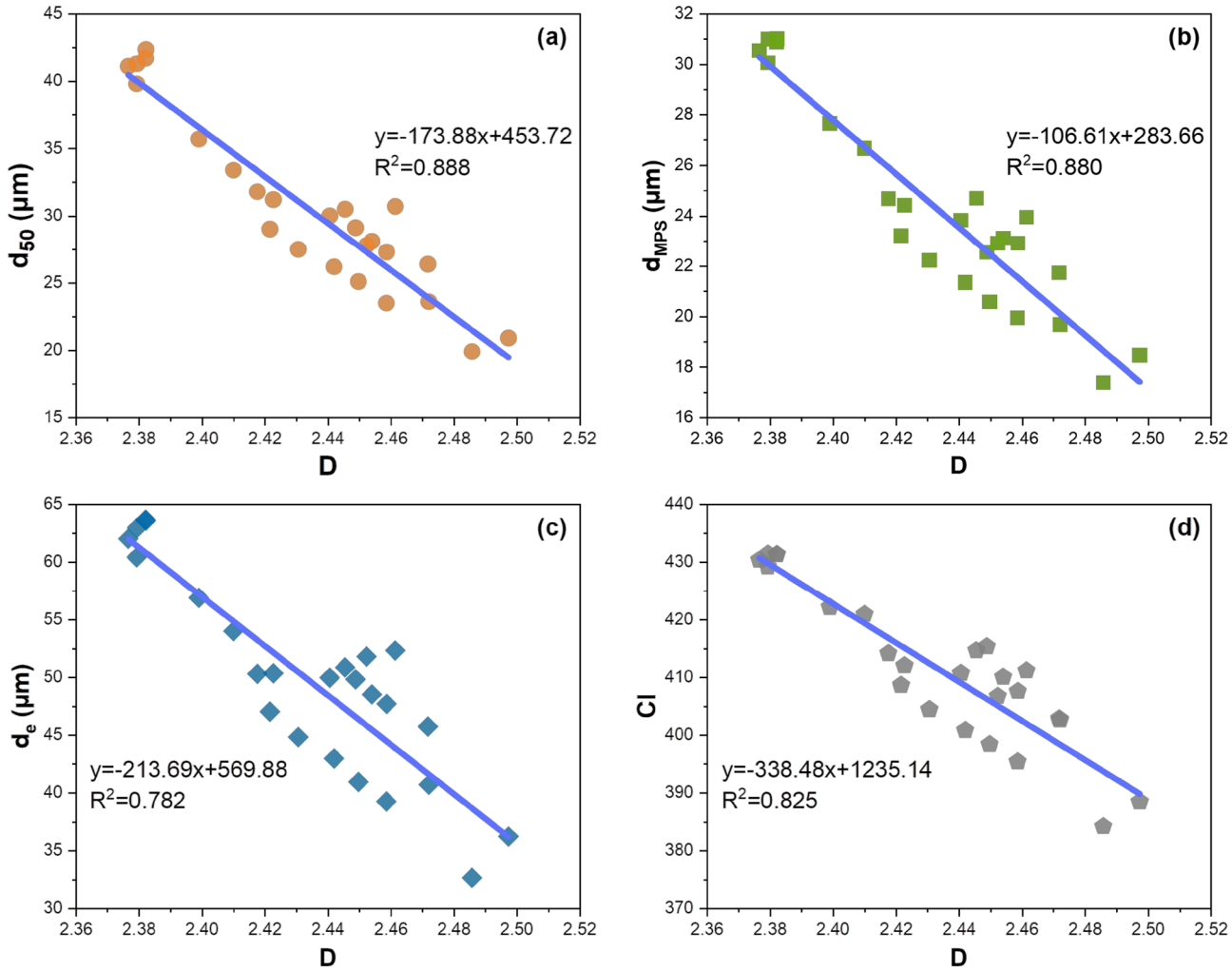

Fig. 4 Relationship between fractal dimension and representative sizes or coarseness index. **a** d_{50} versus D; **b** d_{MPS} versus D; **c** d_e versus D; and **d** CI versus D

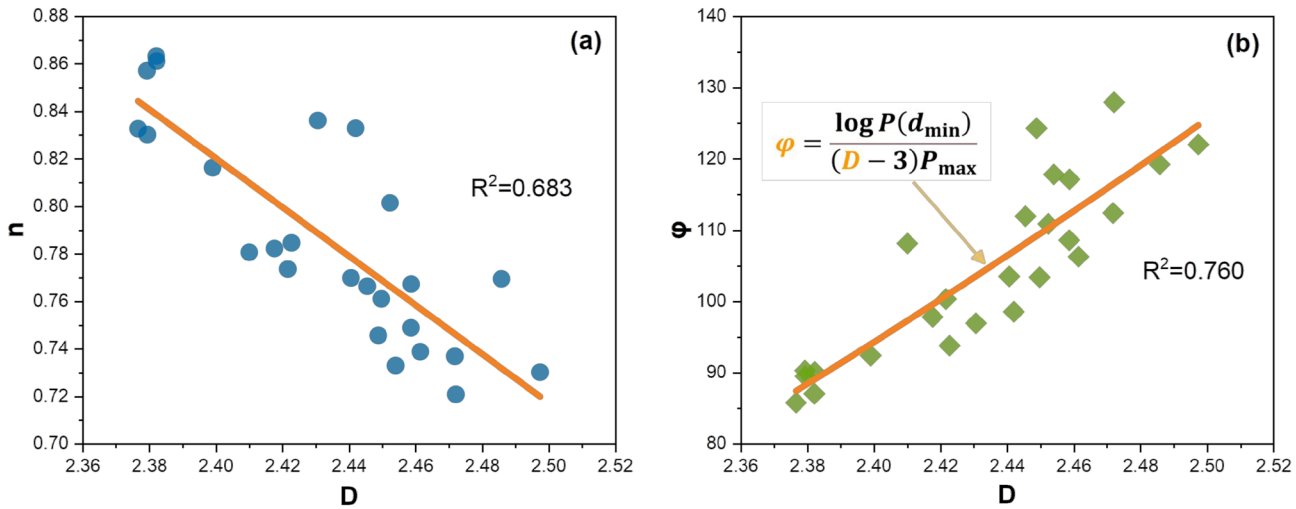

Fig. 5 Relationship between fractal dimension and uniformity and dispersion of PSD. **a** n versus D and **b** φ versus D

characteristic parameters such as representative sizes and distribution uniformity. D describes the size distribution of drilling particles, both qualitatively and quantitatively, and can serve as a state parameter that denotes the degree of breakage of rocks during the drilling process.

4.3 Mechanism of Drilling Particle Generation

In the rock drilling process, drilling particles are produced by rock failure and fragmentation during both the tool–rock interaction and the particle transport processes. The tool–rock interaction can be classified as indentation or cutting depending on the direction of motion of the tool (Huang et al. 2013). Primary particles are produced by rock failure in the zone of tool–rock interaction, and this phenomenon can be concisely defined as the cutting effect. Sequentially, sub-particles are produced by the re-breaking of primary particles in the transport zone, and this is defined as the wear effect.

Following these definitions, cutting and wear effects can be regarded as the primary cause for the generation of drilling particles, and also the two main components consuming breakage energy. The role of the cutting effect is to advance penetration with the cutting effect influencing the rate of penetration (ROP). Meanwhile, wear effects inevitably occur during particles transport and increases the dissipation of energy by abrasion and frictional heat loss. This indicates that a lower degree of wear is conducive to improving the efficiency of rock breakage. Therefore, the predominance of wear effects during the transport process becomes a key concern.

The mechanism of wear is mainly a dynamic effect, including adhesive wear and abrasive wear during the contacting movement of particles (see Fig. 6), while chemical effects (oxidation wear) also occur due to frictional heat release (Bhushan 2002). During the transport process, extrusion and friction occur on the contact surfaces between particles. The particle–particle contact points deform plastically at first, and then cracks initiate and propagate due to the continuous plastic shear action, finally fracturing and with separation then occurring. In this work, both the wear and fracture processes are postulated to follow a shear failure criterion, universally adopted as Mohr–Coulomb theory. Adhesive wear usually occurs when particles have similar surface properties or strong adhesion. Adhesive stress results in the fracture of micro-bulges that protrude on particles and contact during sliding. Abrasive wear usually occurs between hard rough surfaces or on a hard fine particle impacting a soft surface with scrapings separating from the soft surface.

Wear results in finer particles, but it is difficult to distinguish which fine fractions will be produced. In fact, comminution and grinding inevitably cause the loss of surface edges of particles and produces ultrafine particles. Rabinowicz (1995) purposed a calculation of particle sizes produced by wear effect for metallic materials, and that size is estimated in the range of nanometers to tens of microns. Nanometer-scale particles were indeed generated at a volume of ~ 1.88–3.76% in our drilling tests. Such nanometer particles are possibly generated by the surface loss of micron-sized particles, namely as a result of wear effects.

The wear effect is affected by the surface and hydrodynamic properties of the drilling particles, considering the particle transport process. The main influence factors include hardness, restitution coefficient and friction coefficient which depend on mineral types and surface properties, and stress condition of the inter-particle contacts

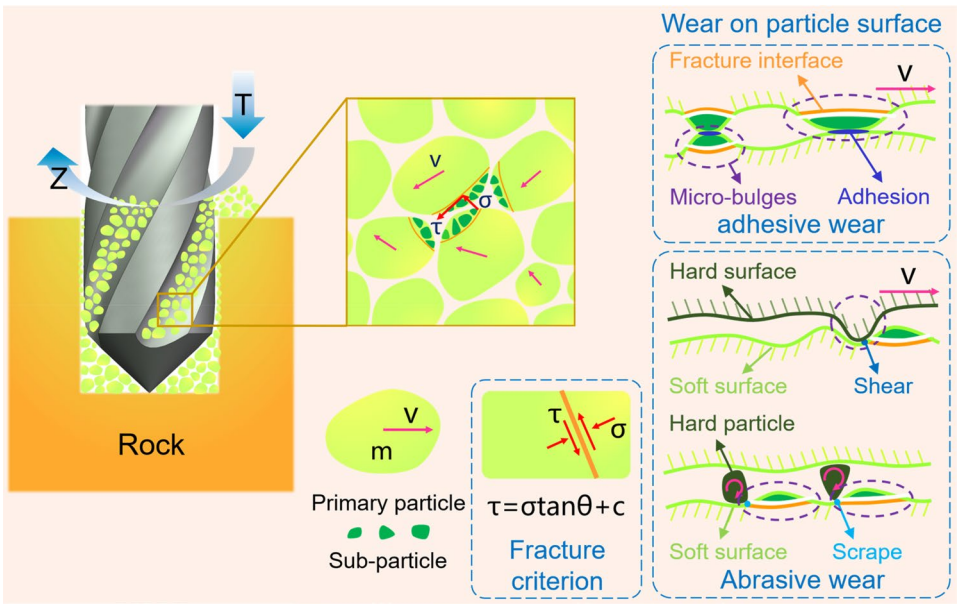

Fig. 6 Schematic diagram of wear effects during transport (v is the velocity of particle, σ and τ are the normal and shear stresses on the fracture plane, θ is the internal friction angle, and c is the cohesion)

and velocity distribution of the particles which are, in turn, affected by drilling operating parameters. It is of engineering signification to investigate the effect of drilling operational parameters on wear effects.

In the transport zone, drilling particles flow in both axial and circumferential directions with the motion of the drill bit and drill rod. The stress conditions present in the granular flows have been extensively studied. A dimensionless number I, also known as Savage number, is used to describe the relative importance of inertia and confining stresses for granular flows (Savage 1984; GDR MiDi 2004),

$$I = \frac{\dot{\gamma} d_p}{\sqrt{P_f \rho_p}}, \tag{15}$$

where $\dot{\gamma}$ is the characteristic shear rate, d_p is the characteristic particle size, P_f is the pressure, namely the normal stress σ, and ρ_p is the bulk density (or volume fraction) of granular flows. ρ_p reflects the space structure of the particles, which is related to the particle size and shape.$\dot{\gamma}$ is defined as

$$\dot{\gamma} = \frac{V_W}{d_p} = \frac{V_W(T, Z)}{d_p}, \tag{16}$$

where V_W is the velocity of the mobile wall. Drilling particles flow in the zone between the wall of hole and drill pipe. Drill pipe can be regarded as a mobile wall which causes shear in granular flows. Therefore, V_W is related to the rate of drill pipe motion, i.e. the rate of penetration T and rotation Z. The effective friction coefficient μ_{eff} is defined as the ratio of the shear stress to the pressure in granular flows

$$\mu_{\text{eff}} = \tau / P_f, \tag{17}$$

where μ_{eff} also reflects the flow property, affected by the dimensionless number I (GDR MiDi 2004). Thus, it is often denoted as $\mu_{\text{eff}}(I)$. I and μ_{eff} are two important parameters of granular flows, reflecting the stress conditions. $\mu_{\text{eff}}(I)$, especially, affects the wear effect directly, considering that the particles are crushed by shear. Therefore, the stress condition or the effective friction coefficient of the granular flow is affected by the rate of penetration and rotation, the loads applied by drill pipe and the bulk density.

Moreover, the velocity distribution within granular flows is complex. It may be similar to the coupled results of plane shear flow (Thompson and Grest 1991) in the direction of axial penetration and annular shear flow (Latzel et al. 2003) in the direction of circumferential rotation. The velocity distribution $u(\vec{r})$ can be expressed as

$$u(\vec{r}) = u(V_W, I, \mu_{\text{eff}}, \vec{r}), \tag{18}$$

where $\vec{r}$ is the position vector. $u(\vec{r})$ is related to V_W, and flowing properties such as I, μ_{eff}. Therefore, the velocity distribution of the drilling particles is somewhat affected by the motion of drill pipe and thus the drilling operational parameters.

4.4 Effect of Operating Parameters on Fractal Dimension

The relationships between drilling operating parameters and PSDs are investigated, with the PSD characterized by a fractal dimension. Figure 7 shows the relationship between fractal dimension and operating parameters. Three distinct levels of D are shown in Fig. 7a. A high fractal dimension, D, (yellow area) can be obtained under low rotation rates, a medium D (green area) under medium rotation rates and low D (blue area) under high rotation rates. Higher D results from lower rotation and penetration rates, with D reaching a maximum of 2.497 for test number of T2Z2.

Figure 7b shows that the correlations between D and penetration rates are inconsistent under different set rates of rotation. D first decreases and then increases with increasing penetration rates under a low rotation rate (Z1). Then D shows a first uptrend then downtrend under medium rotation rates (Z2, Z3 and Z4). While under high rotation rates (Z5), D remains nearly unchanged. This indicates that both penetration and rotation rates have a complex coupled effect on the produced PSDs. It is commonly recognized that the increasing rate of penetration (ROP) tends to increase the particle sizes that are produced. But rotation rate actually affects the flowing properties of the particles and, as a result, the wear effect. These results indicate that rotation exerts a greater effect on wear effect than penetration, since the trends of D depend on the magnitude of Z (low, medium and high level) and even D appears unrelated to penetration rate under high rotation rate.

Figure 7c shows that D generally decreases with an increase in rotation rate, indicating that higher Z can result in an increased proportion of coarse particles with higher uniformity and lower dispersion. A large proportion of coarse particle and an absence of fine particles indicates a low bulk density, which causes less intensive inter-particle contact. This suggests that that a higher rotation rate is conducive to reducing wear effects.

In summary, the PSD of drilling-generated particles is a combined result of cutting and wear effects, while operating parameters of both penetration and rotation rates have coupled effects on the severity of cutting and wear effects. Varying Operating parameters result in various PSDs and its fractal dimensions. Changes in a single rotation or penetration parameter does not result in a corresponding monotonic variation in the fractal dimensions. But larger D or lower

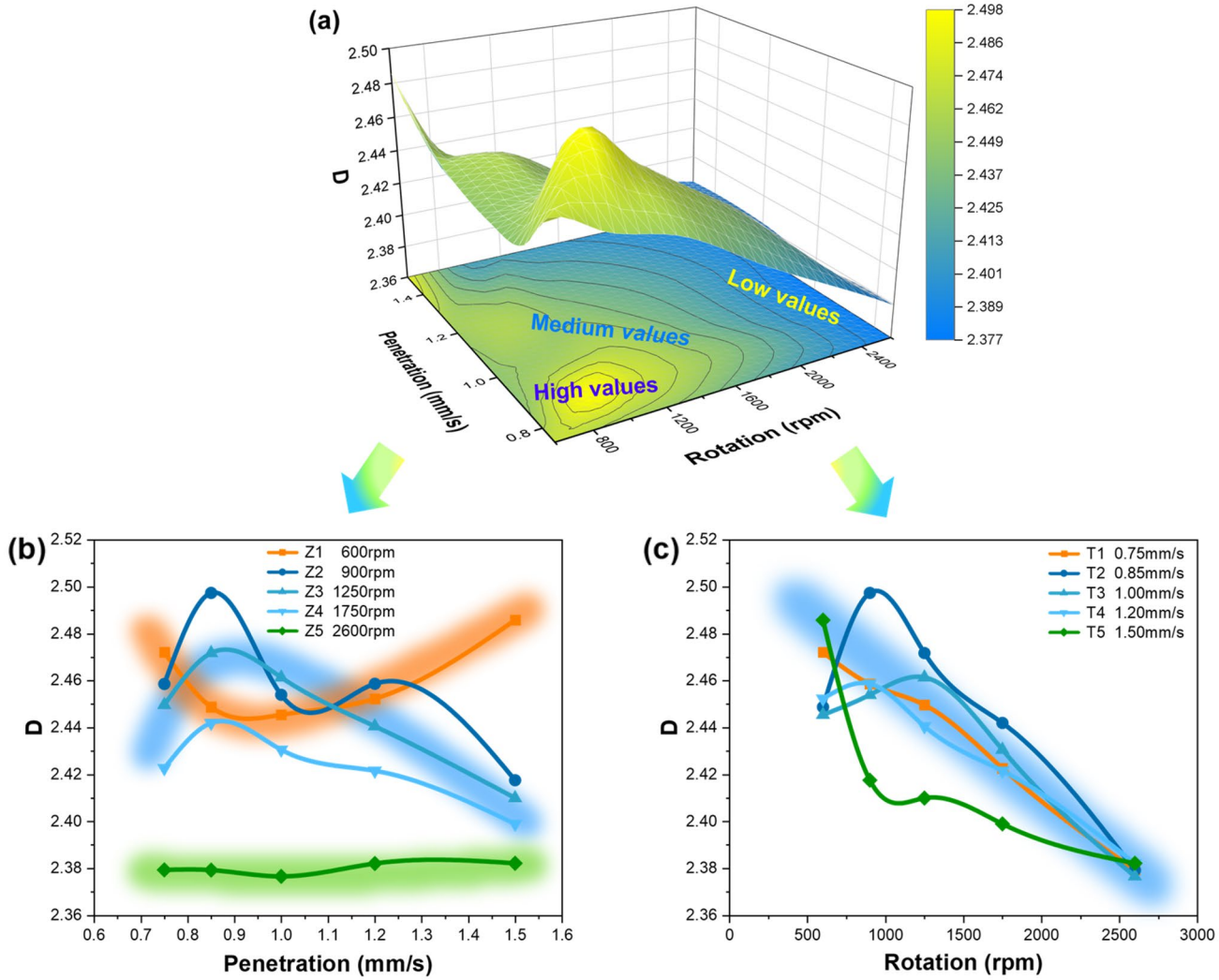

Fig. 7 Relationship between fractal dimension and drilling operational parameters. **a** D for all tests; **b** D versus penetration rate; and **c** D versus rotation rate

wear effects can be obtained at higher rotation rate and this is of advantage in reducing drilling energy consumption.

5 Conclusions

The fractal behavior and characteristic parameters of drilling particle size distribution were analyzed, based on a series of dry drilling tests on shales. The results showed meaningful relationships between drilling PSD and drilling operational parameters. The conclusions are summarized as follows:

The PSDs of the drilling-generated particles conform to both fractal and Rosin–Rammler models. There are significant (linear) negative correlations between fractal dimension and characteristic particle sizes, such as median, mean and absolute particle size. Coarseness index and uniformity are also negatively correlated with fractal dimension. A distributional index, representing dispersion within the PSD, was purposed by considering the triangular-shape of frequency–PSD curve. Dispersion of PSD reflects the span in particle sizes and the maximum frequency of particles, and has a positive correlation with fractal dimension. The results show that fractal dimension describes the size distribution characteristics comprehensively and can be a principal parameter in evaluating the characteristics of the drilling-generated PSD.

The mechanism of production of drilling particles can be generalized as one combining cutting and wear effects. During rock drilling, primary particles are produced by the cutting effect of the tool–rock interaction process, while

sub-particles are produced by wear during subsequent transport process. Two wear mechanisms, namely adhesive and abrasive wear, can cause the re-grinding of primary particles. Thus, wear effects cause the dissipation of energy during particle transport, and need to be weakened to improve drilling efficiency. The severity of the wear effect is related to the stress conditions and the velocity distribution within the granular flow, and affected by drilling operational parameters.

The combined impacts of penetration and rotation have a coupled effect on the cutting and wear process, and thus result in the observed variations in drilling PSDs as reflected in the fractal dimensions. There is a negative correlation between rotation rate and fractal dimension, indicating that higher rotation rate can result in the generation of a larger number of coarse particles and a reduction in wear effects. Thus, increasing the rate of rotation as far as possible is beneficial to improve the energy utilization during cutting and penetration. Overall, for various drilling conditions, the tests on drilling PSDs can indicate optimal settings of operational parameters to improve drilling efficiency.

Funding This work is supported by the National Natural Science Foundation of China (Nos. U21B2072 and 51874310).

Declarations

Conflict of interest We declare that we do not have any commercial or associative interest that represents a conflict of interest in connection with the work submitted.

References

Abu Bakar MZ, Gertsch LS (2013) Evaluation of saturation effects on drag pick cutting of a brittle sandstone from full scale linear cutting tests. Tunn Undergr Sp Tech 34:124–134. https://doi.org/10.1016/j.tust.2012.11.009

Altindag R (2003) Estimation of penetration rate in percussive drilling by means of coarseness index and mean particle size. Rock Mech Rock Eng 36(4):323–332. https://doi.org/10.1007/s00603-003-0002-3

Baumann T, Zunft S (2015) Properties of granular materials as heat transfer and storage medium in CSP application. Sol Energ Mat Sol C 143:38–47. https://doi.org/10.1016/j.solmat.2015.06.037

Bhushan B (2002) Introduction to tribology. Wiley, New York

Blair DP (2004) Curve-fitting schemes for fragmentation data. Fragblast 8(3):137–150

Block G, Jin H (2009) Role of failure mode on rock cutting dynamics. SPE 124870, SPE Annual Technical Conference and Exhibition. New Orleans

Bourrous S, Bouilloux L, Ouf FX, Lemaitre P, Nerisson P, Thomas D, Appert-Collin JC (2016) Measurement and modeling of pressure drop of HEPA filters clogged with ultrafine particles. Powder Technol 289:109–117. https://doi.org/10.1016/j.powtec.2015.11.020

Dahi-Taleghani A, Olson J (2011) Numerical modeling of multistranded-hydraulic-fracture propagation: accounting for the interaction between induced and natural fractures. SPE J 16(3):575–581. https://doi.org/10.2118/124884-PA

Dunatunga S, Kamrin K (2017) Continuum modeling of projectile impact and penetration in dry granular media. J Mech Phys Solids 100:45–60. https://doi.org/10.1016/j.jmps.2016.12.002

Einav I (2007) Breakage mechanics—Part I: theory. J Mech Phys Solids 55(6):1274–1297. https://doi.org/10.1016/j.jmps.2006.11.003

Ersoy A, Waller M (1997) Drilling detritus and the operating parameters of thermally stable PDC core bits. Int J Rock Mech Min Sci 34(7):1109–1123. https://doi.org/10.1016/S1365-1609(97)90203-3

Fang Y, Elsworth D, Wang C, Ishibashi T, Fitts J (2017) Frictional stability-permeability relationships for fractures in shales: friction-permeability relationships. J Geophys Res-Sol Ea 122(3):161–177. https://doi.org/10.1002/2016JB013435

Gamwo K, Kabir A (2015) Impact of drilling fluid rheology and wellbore pressure on rock cuttings removal performance: numerical investigation. Asia-Pac J Chem Eng 10(6):809–822. https://doi.org/10.1002/apj.1917

Gui D, Lei J, Zeng F, Mu G, Zhu J, Wang H, Zhang Q (2010) Characterizing variations in soil particle size distribution in oasis farmlands—a case study of the Cele Oasis. Math Comput Model 51(11–12):1306–1311. https://doi.org/10.1016/j.mcm.2009.10.035

Gupta A, Yan DS (2006) Mineral processing design and operation: an introduction. Elsevier, Netherlands

Hood M, Alehossein H (2000) A development in rock cutting technology. Int J Rock Mech Min Sci 37(1):297–305. https://doi.org/10.1016/S1365-1609(99)00107-0

Huang H, Lecampion B, Detournay E (2013) Discrete element modeling of tool-rock interaction I: rock cutting. Int J Numer Anal Met 37(13):1913–1929. https://doi.org/10.1002/nag.2113

Huang JY, Hu SS, Xu SL, Luo SN (2017) Fractal crushing of granular materials under confined compression at different strain rates. Int J Impact Eng 106:259–265. https://doi.org/10.1016/j.ijimpeng.2017.04.021

Jiang Y, Liu M (2017) Why granular media are thermal, and quite normal after all. Eur Phys J E 40(1):10–26. https://doi.org/10.1140/epje/i2017-11497-4

Krumbein WC (1934) Size frequency distribution of sediments. J Sediment Res 4:65–77

Kwon K, Song C, Park J, Oh J, Lee J, Cho J (2014) Evaluation of drilling effi¬ciency by percussion testing of a drill bit with new button arrangement. Int J Precis Eng Man 15(6):1063–1068. https://doi.org/10.1007/s12541-014-0437-3

Latzel M, Luding S, Herrmann HJ, Howell DW, Behringer RP (2003) Comparing simulation and experiment of a 2D granular Couette shear device. Eur Phys J E Soft Matter 11(4):325–333. https://doi.org/10.1140/epje/i2002-10160-7

Lee B, Toorman E, Fettweis M (2014) Multimodal particle size distributions of fine-grained sediments: mathematical modeling and field investigation. Ocean Dynam 64:429–441. https://doi.org/10.1007/s10236-014-0692-y

Li Y, Weijermars R (2019) Wellbore stability analysis in transverse isotropic shales with anisotropic failure criteria. J Petrol Sci Eng 176:982–993. https://doi.org/10.1016/j.petrol.2019.01.092

Li Y, Jia D, Rui Z, Peng J, Fu C, Zhang J (2017) Evaluation method of rock brittleness based on statistical constitutive relations for rock damage. J Petrol Sci Eng 153:123–132. https://doi.org/10.1016/j.petrol.2017.03.041

Ma J (2015) Review of permeability evolution model for fractured porous media. J Rock Mech Geotech 7(3):119–125. https://doi.org/10.1016/j.jrmge.2014.12.003

McDowell GR, Bolton MD, Robertson D (1996) The fractal crushing of granular materials. J Mech Phys Solids 44(12):2079–2102
MiDi GDR (2004) On dense granular flows. Eur Phys J E 14(4):341–365. https://doi.org/10.1140/epje/i2003-10153-0
Mohammadi M, Khademi Hamidi J, Rostami J, Goshtasbi K (2019) A closer look into chip shape/size and efficiency of rock cutting with a simple chisel pick: a laboratory scale investigation. Rock Mech Rock Eng 53(3):1375–1392. https://doi.org/10.1007/s00603-019-01984-5
Montero E (2005) Rényi dimensions analysis of soil particle-size distributions. Ecol Model 182(3–4):305–315. https://doi.org/10.1016/j.ecolmodel.2004.04.007
Muir Wood D, Maeda K (2007) Changing grading of soil: effect on critical states. Acta Geotech 3(1):3–14. https://doi.org/10.1007/s11440-007-0041-0
Munoz H, Taheri A, Chanda EK (2016) Rock drilling performance evaluation by an energy dissipation based rock brittleness index. Rock Mech Rock Eng 49(8):3343–3355. https://doi.org/10.1007/s00603-016-0986-0
Okorie O (2017) Micromechanical analysis of compaction and drilling of granular media a review. J Geol Geop 6(5):1–4. https://doi.org/10.4172/2381-8719.1000302
Patrik F, Jan K, Milan D, Marek L, Marcel P (2016) Significant damages of core diamond bits in the process of rocks drilling. Eng Fail Anal 59:354–365. https://doi.org/10.1016/j.engfailnal.2015.10.016
Perfect E (1997) Fractal models for the fragmentation of rocks and soils: a review. Eng Geol 48:185–198. https://doi.org/10.1016/S0013-7952(97)00040-9
Rabinowicz E (1995) Friction and wear of Materials. Wiley, New York
Rojek J, Onate E, Labra C, Kargl H (2011) Discrete element simulation of rock cutting. Int J Rock Mech Min Sci 48:996–1010. https://doi.org/10.1016/j.ijrmms.2011.06.003
Rosin P, Rammler E (1933) The laws governing the fineness of powdered coal. J Inst Fuel 7:29–36
Roxborough FF, Rispin A (1973) The mechanical cutting characteristics of the Lower Chalk. Tunnels Tunnell Int 5(1)
Savage SB (1984) Advances in applied mechanics, vol 24. Elsevier, Amsterdam
Simo JC, Ju JW (1987) Strain- and stress-based continuum damage models—I. Formulation. Int J Solids Struct 23(7):821–840. https://doi.org/10.1016/0020-7683(87)90083-7
Steacy SJ, Sammis CG (1991) An automaton for fractal patterns of fragmentation. Nature 353:250–252. https://doi.org/10.1038/353250a0
Thompson P, Grest G (1991) Granular flow: Friction and the dilatancy transition. Phys Rev Lett 67(13):1751–1754. https://doi.org/10.1103/PhysRevLett.67.1751
Turcotte DL (1986) Fractals and fragmentation. J Geophys Res-Sol Ea 91:1921–1926. https://doi.org/10.1029/JB091iB02p01921
Tyler SW, Wheatcraft SW (1992) Fractal scaling of soil particle-size distributions: analysis and limitations. Soil Sci Soc Am J 56(2):362–369. https://doi.org/10.2136/sssaj1992.03615995005600020005x
Wang C, Cheng Y, He X, Yi M, Wang Z (2019) Size effect on uniaxial compressive strength of single coal particle under different failure conditions. Powder Technol 345:169–181. https://doi.org/10.1016/j.powtec.2019.01.017
Wentworth C (1922) A scale of grade and class terms for clastic sediments. J Geol 30(5):377–392. https://doi.org/10.1086/622910
Xu Y (2005) Explanation of scaling phenomenon based on fractal fragmentation. Mech Res Commun 32(2):209–220. https://doi.org/10.1016/j.mechrescom.2003.10.001
Xu Y (2017) The fractal evolution of particle fragmentation under different fracture energy. Powder Technol 323:337–345. https://doi.org/10.1016/j.powtec.2017.10.011
Xu Y (2018) Fractal dimension of demolition waste fragmentation and its implication of compactness. Powder Technol 339:922–929. https://doi.org/10.1016/j.powtec.2018.08.071
Xu Y, Liu S (1999) Fractal character of grain-size distribution of expansive soils. Fractals 7(4):359–366
Xu Y, Wang Y (2017) Size effect on specific energy distribution in particle comminution. Fractals. https://doi.org/10.1142/s0218348x17500165
Xu Y, Song D, Chu F (2016) Approach to the Weibull modulus based on fractal fragmentation of particles. Powder Technol 292:99–107. https://doi.org/10.1016/j.powtec.2016.01.021
Yang X, Wu S, Kang Y, Wang X, Xia R (2014) Pitting mechanism of cemented carbide tool in the early stage of rock drilling. Int J Refract Met H 42:103–107. https://doi.org/10.1016/j.ijrmhm.2013.08.009
Yang X, Nie A, Zhou J (2021) Experimental investigation of the particle size distribution and the influence of operating parameters in limestone drilling. Int J Rock Mech Min Sci. https://doi.org/10.1016/j.ijrmms.2021.104634
Zhang J, Hu Y, Zhang B, Liu Y (2015) Fractal behavior of particle-size distribution during particle crushing of quartz sand and gravel. Chinese J Geotech Eng 37(5):784–791. https://doi.org/10.11779/CJGE201505003
Zhao W, Cui Z, Hong M (2017) Fractal features of soil particle-size distributions and their relationships with soil properties in gravel-mulched fields. Arab J Geosci. https://doi.org/10.1007/s12517-017-3008-y
Zhou W, Han Y, Li Y, Yang J, Ma S, Sun Y (2019) Research on prediction model of ore grinding particle size distribution. J Disper Sci Tech 41(4):537–546. https://doi.org/10.1080/01932691.2019.1592688

Publisher's Note Springer Nature remains neutral with regard to jurisdictional claims in published maps and institutional affiliations.